

# RF MEMS Based Half Mode Bowtie Shaped Substrate Integrated Waveguide Tunable Bandpass Filter

Muhammad Z. Ur Rehman<sup>1, 2</sup>, Zuhairi Baharudin<sup>1, \*</sup>, Mohd A. Zakariya<sup>1</sup>,  
Mohd H. M. Khir<sup>1</sup>, Muhammad T. Jilani<sup>1</sup>, and Muhammed T. Khan<sup>1</sup>

**Abstract**—A tunable planar bandpass filter based on a technique that utilizes a half mode substrate integrated waveguide (HMSIW) and novel inter-resonator coupling is presented. The tunable HMSIW based bandpass filter is implemented using two half triangle shaped cavities coupled together through inter-resonator coupling forming half mode bowtie shaped structure. The bowtie-shaped filter exhibits similar performance as found in rectangle- and circle-shaped SIW based bandpass filters. This concept reduces the circuit foot print, and miniaturization high quality factor is maintained by the structure. The tunable filter utilizes packaged RF MEMS switches; switching between different configurations of switches achieves four distinctive frequency states between 4.8–5.3 GHz. The filter maintains a constant absolute 1 dB bandwidth of  $100 \pm 10$  MHz for all frequency states.

## 1. INTRODUCTION

Filters have received particular attention with the advent of various wireless systems, and interest has dramatically increased with the introduction and development of new millimeter waves applications over the past decade. Various applications have been recently proposed including wireless local area networks [1], radars [2], intelligent transportation systems [3] and imaging sensors [4]. Efficient filters demand has also increased with the development of chip-sets operating at 60 GHz or even higher frequencies by a number of semiconductor industries [5].

Filters based on Substrate Integrated Waveguide (SIW) structures are achieved through incorporating the rectangular waveguide structure into the microstrip substrate [6]. SIWs are dielectric filled and are formed from the substrate material utilizing two rows of conducting vias connecting bottom and top metal plates. These vias are embedded in dielectric filled substrate, hence providing easy combination with other planar circuits and reduction in size. The size reduction along with involving dielectric filled substrate instead of air-filled reduces quality factor ( $Q$ ), but the entire circuitry including waveguide and microstrip transitions can be realized by using printed circuit board (PCB) technology or other techniques, such as LCP [7] and LTCC [8].

Circular and rectangular cavities have been due to the design methodologies adopted based on air filled waveguides. Various SIW filters structures have been proposed in the literature; however there still exists a need to further miniaturize the structure. Furthermore, the cavities are only in either circular or rectangular shape; therefore, a triangle-shaped cavity will reduce the circuit footprint. In this paper, triangle-shaped waveguide is proposed for its ability to miniaturize the cavity size.

Hong et al. in 2006 proposed a half-mode substrate integrated waveguide (HMSIW) concept which can reduce the size of SIW components by half [9]. Performances at microwave and millimeter wave bands show that its attenuation is less than that of planar microstrip and SIW. Thus, further

---

*Received 14 September 2015, Accepted 9 November 2015, Scheduled 23 November 2015*

\* Corresponding author: Zuhairi Baharudin (zuhairb@petronas.co.my).

<sup>1</sup> Department of Electrical and Electronics Engineering, Universiti Teknologi PETRONAS, Tronoh, Perak, Malaysia. <sup>2</sup> Department of Physics, COMSATS Institute of Information Technology, Park road, Islamabad, Pakistan.

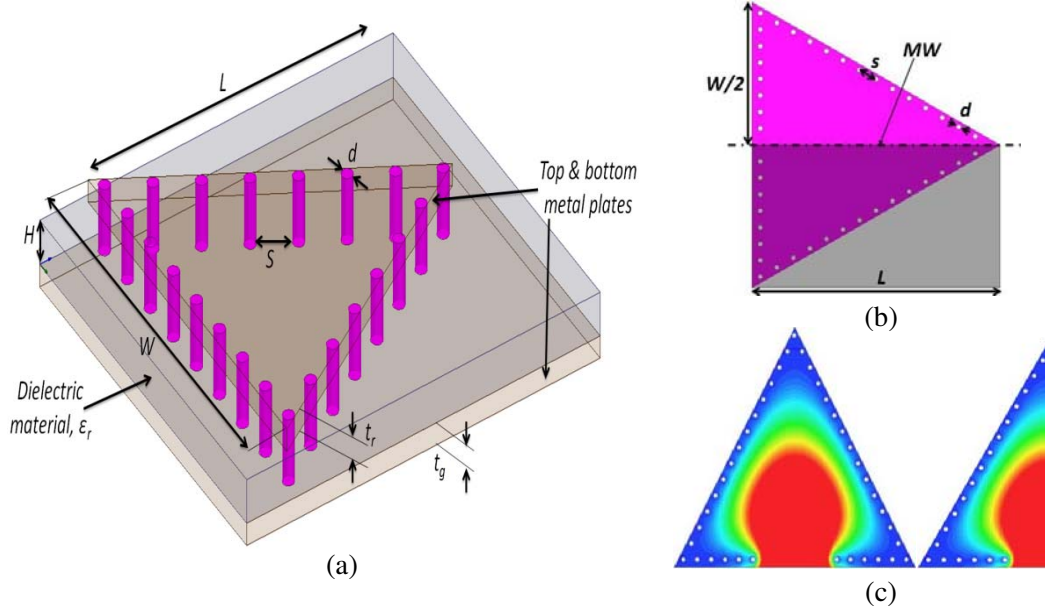


**Figure 1.** (a) Triangular SIW resonator, (b) HMSIW resonator structure, (c) SIW and HMSIW cavity dominant modes.

compression can be brought to the size of a microwave or millimeter wave integrated circuit based on these wave structures.

The structure of an SIW and HMSIW and the dominant modes are shown in Figure 1. An HMSIW is obtained through placement of an open circuit along the symmetric plane in the transmission direction, thus half of the SIW will keep the half-field distribution unchanged if cutting plane is a Magnetic Wall (MW). The open side aperture of the HMSIW is nearly equivalent to a perfect MW due the high ratio of width to height, and it has been shown that HMSIW retains low loss characteristics obtained through SIW structures.

In this paper, a bowtie-shaped HMSIW resonator based bandpass filter is presented. This resonator structure is a miniaturized form of SIW cavity and exhibits similar low-loss and high quality characteristics as found in its other counterparts. The bowtie-shaped HMSIW bandpass filter is designed into a tunable filter, utilizing additional inductive via posts connecting/disconnecting the bowtie-shaped HMSIW resonators with onboard RF MEMS switches. A total of four distinctive frequency states between 4.8 and 5.3 GHz are achieved for the designed tunable bandpass filter, and the filter has onboard bias circuitry to actuate the RF MEMS switches. In addition, detailed design steps and coupling mechanisms are discussed. The proposed filter is compact and suitable for integration with planar devices, and its small footprint area allows other devices to be easily integrated on a single board.

## 2. HALF MODE BOWTIE SHAPED SIW RESONATOR DESIGN

The SIW and HMSIW resonators and their electric field distributions are shown in Figure 1. The width  $W$  Length  $L$  of the SIW resonator along with the diameter of vias  $d$  and separation between two vias  $s$  control the resonance frequency, whereas in the case of HMSIW, the resonator width is reduced to half of the width of a SIW resonator denoted as  $W/2$ .

The design and implementation of HMSIW filters follow the same design principles of an SIW resonator structure. The most common technique is to form the SIW cavity through metallic sidewalls [10] as shown in Figure 1(a). A dielectric substrate having width of  $h$  forms the resonator, and the resonator is of length  $L$ . The bottom and top of the resonator are constructed through placing metallic plates and conducting posts/vias going through the substrate connects the top and bottom plates, hence forming the sidewalls of the cavity. The choice of diameter and separation between the two vias forms the basis of the SIW filters, which, therefore, should be selected in a manner that

minimum radiation loss is exhibited.

The Dealandes and Wu [10] study reveals two primary design rules for SIW structures as given in (1); these rules are followed in order to ensure same design and modeling methodology adopted for rectangular waveguides. These rules pertain to the diameter  $d$  of the via posts and the via post spacing  $s$ :

$$d < \frac{\lambda_g}{5} \quad (1)$$

$$s \leq 4d \quad (2)$$

In our design,  $d$  and  $s$  are chosen to be 0.8 mm and 2 mm, respectively. These values ensure less radiation loss, and the SIW cavity acts closely to a rectangular waveguide. For the TE<sub>101</sub> mode, the dimensions of the SIW resonator structure are calculated by using the relation in Eq. (3).

$$f_{\text{TE}_{101}} = \frac{c}{2\sqrt{\mu_r \epsilon_r}} \sqrt{\left(\frac{1}{W_{\text{eff}}}\right)^2 + \left(\frac{1}{L_{\text{eff}}}\right)^2} \quad (3)$$

The notations  $W_{\text{eff}}$  and  $L_{\text{eff}}$  denote effective width and length of the SIW resonator, respectively:

$$W_{\text{eff}} = W - \frac{d^2}{0.95s}; \quad L_{\text{eff}} = L - \frac{d^2}{0.95s} \quad (4)$$

where  $W$  and  $L$  are the real width and length of the SIW resonator, and  $c$  is the velocity of light in free space. In this design, the width and length of the triangular resonator structure is computed using Eqs. (3) and (4) as shown in Figure 1. Utilizing this method, the cavity is designed for the specifications laid out in Table 1.

**Table 1.** Design specifications of the bandpass filter.

Key Parameters	Values
Passband Centre Frequency	4.8 GHz
Passband Return Loss, $S_{11}$	< -25 dB
Passband Insertions Loss, $S_{21}$	> -2 dB
Passband Bandwidth at -3 dB	> 300 MHz
Stopband rejection	> 30 dB

The triangle-shaped resonator and subsequent bowtie-shaped two-pole filter are designed using Roger RT/Duriod 5880 material substrate having dielectric constant of 2.2 and substrate height of 787  $\mu\text{m}$ . Theoretically, the resonance frequency does not depend on the thickness of the substrate. However, it has been observed in literature that it does play a role on the loss (mainly on radiation loss). The thicker the substrate is, the lower the loss or higher  $Q$  is. It has been shown that a slight increase or decrease in the substrate thickness changes the unloaded quality factor.

### 2.1. Novel Inter-Resonator and Input-Output Coupling

The two-pole bandpass HMSIW filter is accomplished by means of coupling two half-mode triangular resonators designed for a specific resonant mode. The inter-resonator coupling design methodology closely resembles conventional simulation-based microstrip filters design. In this novel coupling, three individual resonant lengths are placed as inter-resonator coupling lengths used to couple the two resonators as shown in Figure 2. The RF input and output microstrip-to-SIW transitions attached to the two single cavity resonators provide the RF input and output coupling, the corresponding dimensions of both the couplings are listed in Table 2.

$$M_{1,2} = \frac{\text{FBW}}{\sqrt{g_1 g_2}}, \quad Q_{e1} = \frac{g_0 g_1}{\text{FBW}}, \quad Q_{e2} = \frac{g_2 g_3}{\text{FBW}} \quad (5)$$

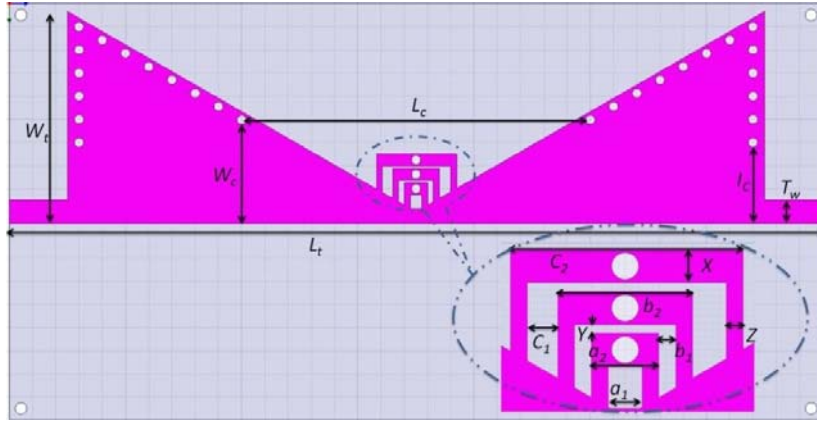


**Figure 2.** Bowtie shaped two pole bandpass filter dimensions.

The inter-resonator coupling and input-output couplings for the two-pole bandpass filter depicted in Figure 2 are computed based on the external quality factor and coupling coefficients from Eq. (5); these derived expressions are based on lowpass prototype parameters [11], where FBW is the fractional bandwidth, and  $g_0, g_1, g_2, g_3$  are the Chebyshev lowpass prototype values used to calculate the external quality factors  $Q_{e1}$  and  $Q_{e2}$ , and mutual coupling coefficient denoted as  $M_{1,2}$ . The mutual coupling coefficient  $M_{1,2}$  computed based on second order Chebyshev response prototype parameters is compared with simulated one obtained through weak coupling, whereas the theoretical external coupling coefficient's values are then compared with the external quality factor obtained through simulations based on expression given in Eq. (6).

The inter-resonator dimensions are primarily dependent on three parameters: the coupling opening length denoted as  $L_c$ , the coupling opening width  $W_c$ , and the spacing among three resonant lengths given as  $a_1, b_1$  and  $C_1$ . For 0.01 dB passband ripples and fractional bandwidth of 0.05 as listed in Table 1, expression (5) results in values of  $M_{1,2} = 0.116$  and  $Q_{e1} = Q_{e2} = 8.97$ . Consequently, the widths of  $L_c$  and  $W_c$ , and separation among three resonant lengths are selected from closely matched coupling coefficient values based on the external quality factor in Eq. (6). The values obtained through various combinations of the dimensions are depicted in Figure 3.

$$Q_{ext} = \frac{f_0}{\Delta f_{-3dB}} \quad (6)$$

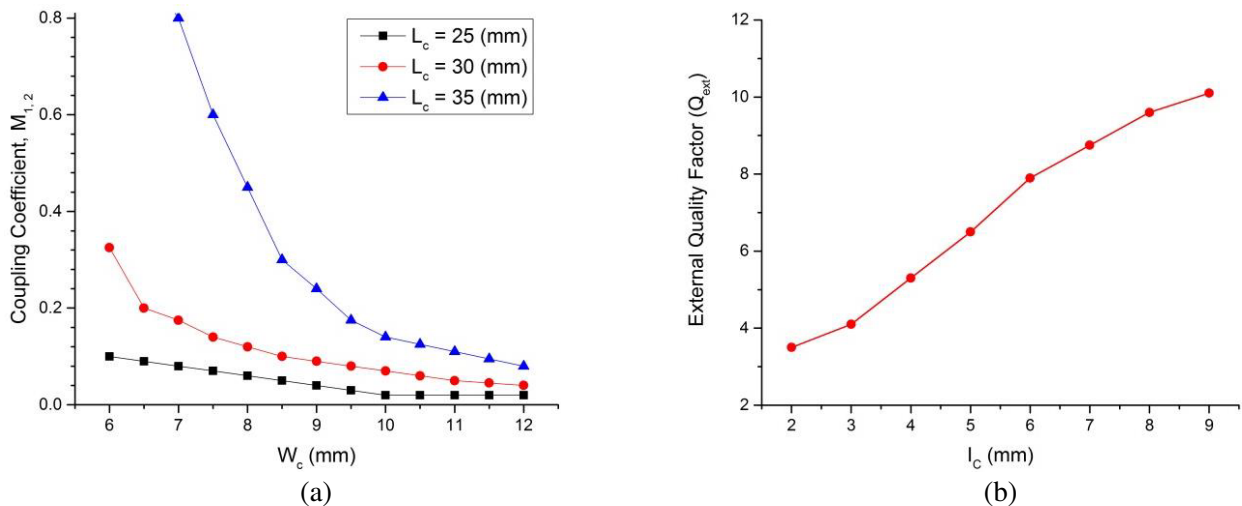


**Figure 3.** (a) Inter-resonator coupling dimensions extracted, (b) input-output coupling width.

The microstrip to SIW transitions at the input and output ports are of width  $T_w$ , and the dimensions of the feed lines are computed through transmission line calculator. However, the input and output coupling openings denoted as  $I_c$  are selected as a result of comparison of the simulated extracted external quality factors computed through Eq. (6) and external quality factors calculated on basis of theoretical LPF prototype parameters as given in Eq. (5). These values are then compared to the simulated extracted external quality factors and coupling coefficients for a particular cavity geometry. Iterations and adjustments to the dimensions of the coupling areas of the filter are performed until the calculated values match the extracted values from full-wave simulation, providing the desired filter. All the finalized dimensions of the filter are listed in Table 2, whereas the resulting bandpass filter is fabricated to validate the simulated design and measure the performance. The fabricated filter is shown in Figure 4.

**Table 2.** Bandpass filter parameter’s dimensions and descriptions.

Key Parameters	Value (mm)	Description	Key Parameters	Value (mm)	Description
$W_t$	19.0	Bowtie filter full width	$L_c$	30.0	Coupling opening length
$L_t$	70.0	Bowtie filter full length	$W_c$	8.95	Coupling opening width
$L$	30.0	Resonator’s Length	$X, Y, Z$	1.0, 1.25, 0.5	Inter-resonator dim
$W/2$	17.5	Resonator’s Width	$C_2, C_1$	6.9, 0.9	Inter-resonator dim
$I_c$	7.0	I/O coupling	$b_2, b_1$	4.0, 0.5	Inter-resonator dim
$T_w$	2.0	Transition Width	$a_2, a_1$	2.0, 1.0	Inter-resonator dim

### 2.2. Tunable Structure and Bias Circuitry

The HMSIW is tuned through connecting/disconnecting inductive via posts using RF MEMS switches. The tuning network as shown in Figure 5 is composed of four vias, and each via is connected through a section of transmission line to the HMSIW resonator. On the other hand, a Single Pole Dual Throw (SPDT) RADANT RMSW221 RF MEMS switch is attached to two transmission lines connecting each HMSIW resonator [12]. The four switches ( $S1, \dots, S4$ ) configurations as listed in Table 3 are used to yield four distinctive frequency states.

The Source ( $S$ ) to Load ( $L$ ) tuning network comprises four distinct inductors employed through connecting short sections of transmission line in series with vias, these added inductances are switchable through RF MEMS switches  $S1$  to  $S4$ . The design of the tunable filter is achieved through two tuning branches with switchable vias connected to each resonator. Consequently, switching on/off the two SPDT RF MEMS switches connects/disconnects each transmission line with via from the HMSIW resonator, hence adding inductance to the resonator shifts the frequency. The dimensions of all the tuning network elements and distance from  $S$  and  $L$  are depicted in Figure 5.

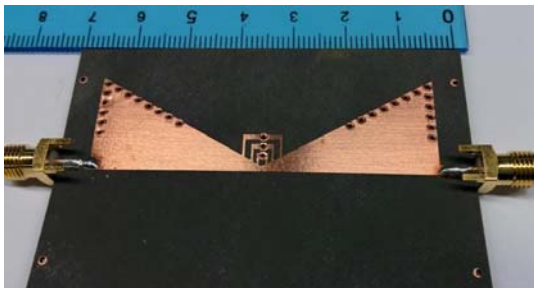


**Figure 4.** Fabricated static bowtie shaped two pole bandpass filter.

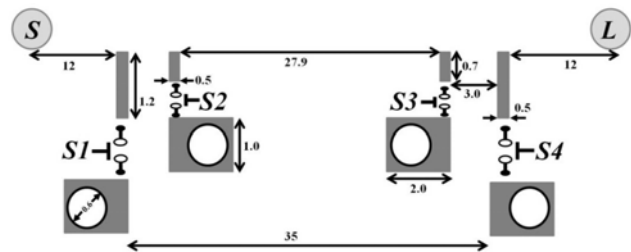


**Figure 5.** Tuning network of the HMSIW bandpass filter from source to load.

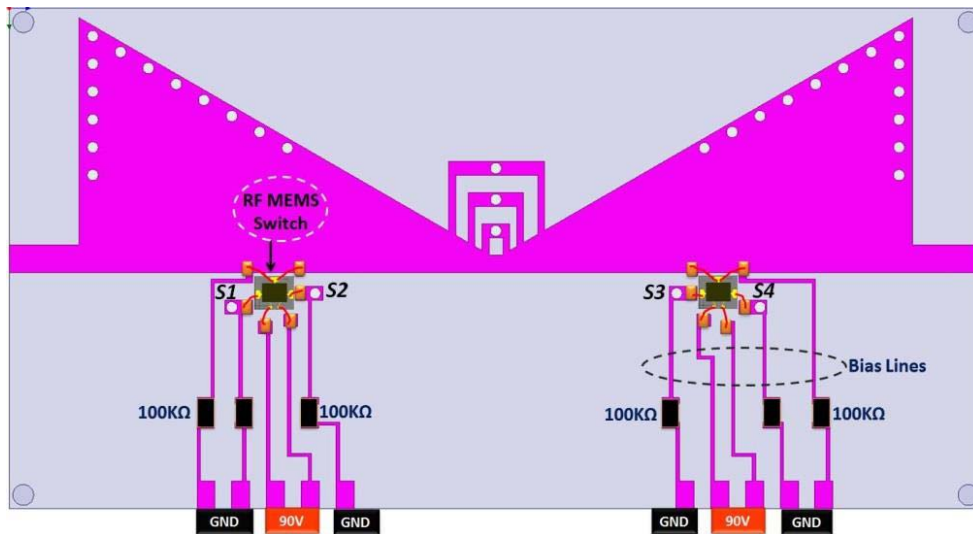
**Table 3.** Tuning configurations (0: Open; 1: Closed).

Config.	S1S2S3S4	Resonant Frequency
1	0000	4.85 GHz
2	1001	5.00 GHz
3	0110	5.15 GHz
4	1111	5.30 GHz

The implementation of the tunable HMSIW resonator based bandpass filter along with the operational diagram of the RF MEMS switches actuated through the onboard bias circuitry is shown in Figure 6. The proposed tuning structure is attached to the open end of the bowtie shaped HMSIW structure. The positioning of the transmission lines and vias together with the RF MEMS is selected so that maximum tuning is achievable. The transmission lines, vias, and RF MEMS switches operation are all simulated and optimized using HFSS, and the resonator layout with the placement of RF MEMS switches is also optimized to meet tuning specifications. The optimization is such that equally-spaced resonant frequencies are obtained using various combinations of the switches, and the  $s$ -parameters of the RF MEMS switches in both the up and down states are considered during optimization.

As depicted in Figure 6, both the RF MEMS SPDT switches are composed of two separate gates and drains, whereas a common source is used to connect/disconnect transmission lines with the inductive via posts. An on state of the switch refers to connecting the transmission line to the via, whereas the off state refers to disconnecting the via post from the resonator. The states are selected in a way that the highest frequency is achieved when all the vias are connected, and the lowest frequency is when all are in the off state. Although  $16(4^2)$  configurations can be achieved by the combination of the switches, only four distinct frequency states were achieved through full-wave simulations in HFSS.

The onboard bias circuitry has switches placed on pads created on top of the board beneath the resonators; the pads are wire-bonded to the gate, drain and source of the RF MEMS switches. Each gate of the RF MEMS switch is actuated by applying a voltage of 90 V, while GND is connected through 100 Kohm resistors to the drain and source of the switch. The bias lines of 0.5 mm thickness with spacing of 1.5 mm are placed on the board to actuate the RF MEMS switches.

**Figure 6.** Functionality of the bowtie shaped tunable two pole HMSIW bandpass filter.

### 3. RESULTS AND DISCUSSIONS

The simulations to obtain the filter responses from the designed structures are conducted using ANSYS High Frequency Structure Simulator (HFSS). In addition, Agilent Vector Network Analyzer (VNA) is utilized for the measurements of the fabricated filters.

The static bowtie-shaped HMSIW bandpass filter is designed by the specifications shown in Table 1, and its corresponding design structure displayed in Figure 2 is realized with the fabricated unit displayed in Figure 4 and responses shown in Figure 7. The simulated  $S_{21}$  and  $S_{11}$  response of the bowtie shaped bandpass filter shown in Figure 7(a) reveals that the  $S_{11}$  value at the center frequency of 4.8 GHz is less than  $-20$  dB, whereas the  $S_{21}$  response is greater than  $-2$  dB, and the passband bandwidth at  $-3$  dB is greater than 250 MHz. On the other hand, the measured  $S_{21}$  response at the center frequency of 4.8 GHz is better than  $-2.7$  dB, and its corresponding  $S_{11}$  response at the center frequency is less than  $-15$  dB, as depicted in Figure 7(b). However, the passband bandwidth at 3 dB is greater than 200 MHz.

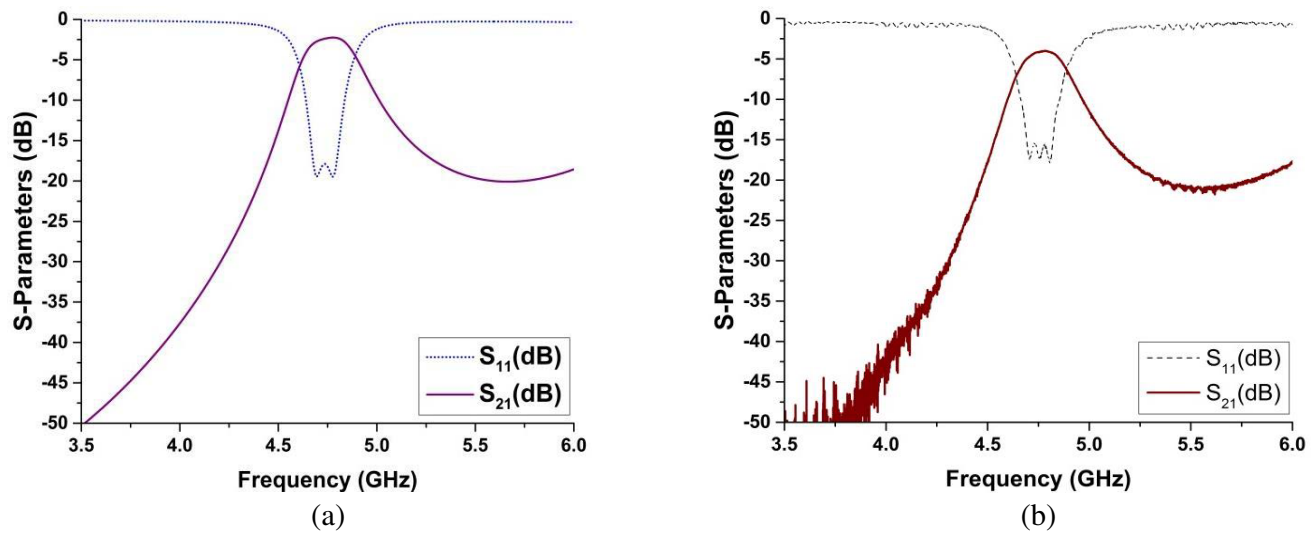


**Figure 7.** (a) Simulated, (b) measured response of the static bowtie shaped HMSIW filter.

The desired bowtie-shaped HMSIW tunable filter with the added transmission lines coupled with vias as shown in Figure 6 is realized with the simulated and measured responses as shown in Figure 8(a) and Figure 8(b), respectively. The simulated response of the two-pole tunable filter depicts four distinctive resonant frequencies states of 4.85, 5.0, 5.15 and 5.30 GHz for the switches configurations of 0000, 1001, 0110 and 1111, respectively. The tuning branches provide the largest frequency shift (i.e., of 5.30 GHz) when all the lines are connected to the vias; it is primarily because all the transmission lines are of small inductance values. Similarly, the other two frequency shifts of 5.0 and 5.15 GHz occur when at both the resonators with exactly the same distances the transmission lines are connected to their respective vias, i.e., switches ( $S_2, S_3$ ) and ( $S_1, S_4$ ) are connected. However, when all the switches are kept open, the tunable filter resonates at the frequency of 4.85 GHz. The simulated insertion and return losses are better than  $-2.6$  dB and 38 dB, respectively, for all states. The passband bandwidth at 3 dB and 1 dB for all the frequency states is observed to be greater than 250 MHz and 150 MHz, respectively.

The measured insertion and return losses of the bowtie-shaped HMSIW tunable filter for all the four frequency states are shown in Figure 8(b). The measured absolute 1 dB and 3 dB bandwidths for all the frequency states vary between  $100 \pm 10$  MHz and  $175 \pm 25$  MHz, respectively. The measured return losses, midband insertion losses, absolute 1 dB and 3 dB bandwidths in terms of frequency states achieved are listed in Table 4. The measured responses show similar trends in terms of frequency tuning between the four tuning states modes as observed in the simulated responses. It can be observed that as the frequency increases with respect to number of switches that are closed, the insertion loss also decreases

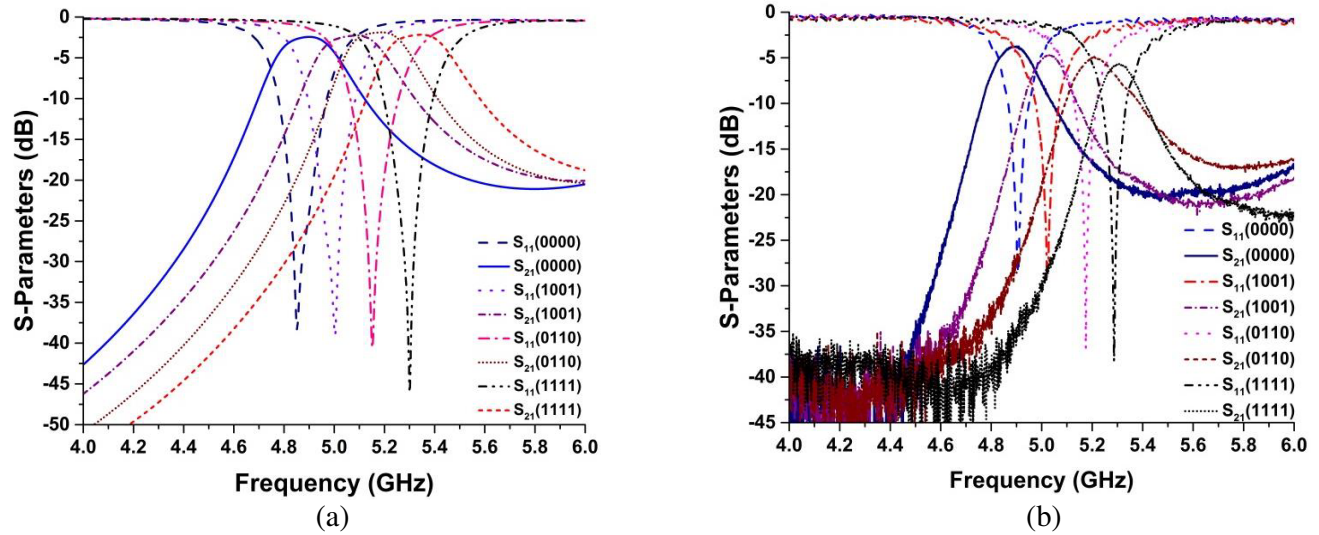


Figure 8. (a) Simulated, (b) measured insertion & return losses of the bowtie shaped tunable filter.

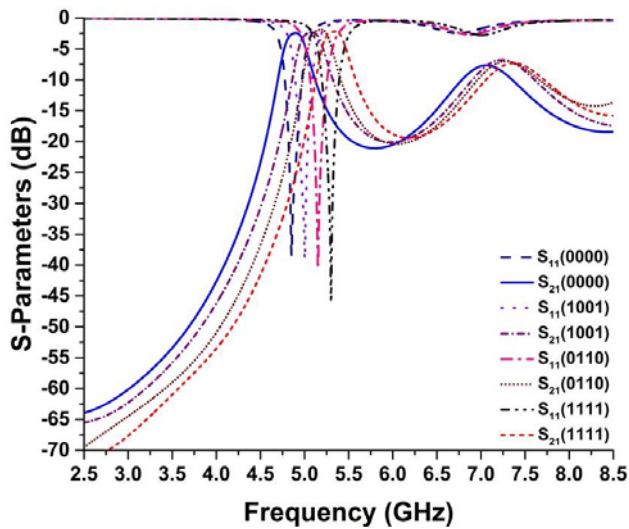


Figure 9. Wideband response of the tunable bowtie shaped two pole bandpass filter.

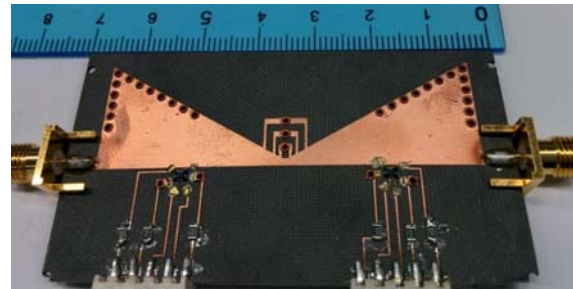


Figure 10. Fabricated RF MEMS tunable bowtie shaped two pole bandpass filter.

due to added resistances of the closed RF MEMS switches. A notable difference has been observed in the simulated and measured bandwidths; the measured bandwidths are narrower than the bandwidths achieved through simulations, hence presenting better quality factor in terms of the bandwidths.

The wideband response of the tunable filter for all tuning states is shown in Figure 9, and a stopband rejection greater than 20 dB can be observed from 5.4 to 6.2 GHz. The first spurious resonances for all the states are further beyond 7.0 GHz. The upper passband produced due to cancellation of the  $TE_{101}$  and  $TE_{201}$  modes is distanced enough from the filter passband, hence a pure Chebyshev response is observed as the design is based on Chebyshev LPF prototype parameters. However, the measured insertion losses mainly include the losses due to the wire-bonding of the RF MEMS switches to the copper pads, the gold wire-bonding required added pads of gold on top of the copper pads, hence adding losses to the filter. The additional gold patches and the wire-bonded RF MEMS switches are shown in the fabricated unit displayed in Figure 10.

**Table 4.** Summary of tunable bandpass filter performance.

Key Parameters	State 0000		State 1001	
	Simulated	Measured	Simulated	Measured
Passband Centre Frequency (GHz)	4.85	4.90	5.0	5.02
Passband Return Loss, $S_{11}$ (dB)	37.95	28.64	38.14	29.07
Passband Insertions Loss, $S_{21}$ (dB)	$> -2.61$	$> -3.74$	$> -2.60$	$> -4.65$
Passband Bandwidth at $-3$ dB level	0.26 GHz	0.18 GHz	0.29 GHz	0.16 GHz
Passband Bandwidth at $-1$ dB level	0.16 GHz	0.1 GHz	0.18 GHz	0.08 GHz
Key Parameters	State 0110		State 1111	
	Simulated	Measured	Simulated	Measured
Passband Centre Frequency (GHz)	5.15	5.17	5.30	5.28
Passband Return Loss, $S_{11}$ (dB)	39.96	36.94	45	38.25
Passband Insertions Loss, $S_{21}$ (dB)	$> -1.98$	$> -4.90$	$> -2.32$	$> -5.64$
Passband Bandwidth at $-3$ dB level	0.26 GHz	0.2 GHz	0.28 GHz	0.15 GHz
Passband Bandwidth at $-1$ dB level	0.17 GHz	0.1 GHz	0.18 GHz	0.09 GHz

#### 4. CONCLUSION

A tunable half-mode bowtie-shaped bandpass filter based on RF MEMS switches utilizing triangular structure HMSIW is proposed in this paper. The filter exhibits good performance, and a miniaturized version of the SIW structure is exploited in the design process. The tunable filter is unique in terms of the tuning mechanism and the coupling between the HMSIW resonators. The RF MEMS switchable bandpass filter is designed, simulated and fabricated. The measured filter response shows four distinct frequency states between 4.85 to 5.3 GHz at constant intervals of 0.15 GHz with a nearly constant 3 dB bandwidth of  $175 \pm 25$  MHz. The simple structure of the filter allows easy integration with planar circuits and devices.

#### ACKNOWLEDGMENT

This work was supported by the Fundamental Research Grant Scheme (FRGS) of Ministry of Higher Education, Malaysia. The authors would like to thank Dr. John Ojur Dennis and his student Dr. Farooq Ahmed of Nano fabrication facility in Universiti Teknologi PETRONAS, Malaysia for providing their guidance and wire-bonding facility.

#### REFERENCES

1. James, J., P. Shen, A. Nkansah, X. Liang, and N. J. Gomes, "Millimeter-wave wireless local area network over multimode fiber system demonstration," *IEEE Photonics Technology Letters*, Vol. 22, 601–603, 2010.
2. Wang, L., S. Glisic, J. Borngraeber, W. Winkler, and J. C. A Scheytt, "Single-ended fully integrated SiGe 77/79 GHz receiver for automotive radar," *IEEE Journal of Solid-State Circuits*, Vol. 43, 1897–1908, 2008.
3. Yan, X., H. Zhang, and C. Wu, "Research and development of intelligent transportation systems," *Proceedings of the 11th International Symposium on Distributed Computing and Applications to Business Engineering & Science*, 321–327, Guilin, China, 2012.
4. Wilson, J. P., C. A. Schuetz, R. Martin, T. E. Dillon, P. Yao, and D. W. Prather, "Polarization sensitive millimeter-wave imaging sensor based on optical up-conversion scaled to a distributed

- aperture,” *Proceedings of the 37th International Conference on Infrared, Millimeter, and Terahertz Waves*, Vol. 1, 23–28, Wollongong, Australia, 2012.
5. Niknejad, A. M. and H. Hashemi, *Millimetre-wave Silicon Technology: 60 GHz and Beyond*, Springer, 2008.
  6. Hirokawa, J. and M. Ando, “Single-layer feed waveguide consisting of posts for plane TEM wave excitation in parallel plates,” *IEEE Transactions on Antennas and Propagation*, Vol. 46, No. 5, 625–630, 1998.
  7. Yang, K. S., S. Pinel, K. Kim, and J. Laskar, “Low-Loss integrated-waveguide passive circuits using liquid-crystal polymer System-on-Package (SOP) technology for millimeter-wave applications,” *IEEE Transactions on Microwave Theory and Techniques*, Vol. 54, No. 12, 4572–4579, 2006.
  8. Xu, J., Z. N. Chen, X. Qing, and W. Hong, “140-GHz planar broadband LTCC SIW slot antenna array,” *IEEE Transactions on Antennas and Propagation*, Vol. 60, No. 6, 3025–3028, 2012.
  9. Hong, W., B. Liu, and Y. Q. Wang, “Half mode substrate integrated waveguide: A new guided wave structure for microwave and millimeter wave application,” *IRMMW-THz Conference Digest*, 219, 2006.
  10. Deslandes, D. and K. Wu, “Accurate modeling, wave mechanisms, and design considerations of a substrate integrated waveguide,” *IEEE Transactions on Microwave Theory and Techniques*, Vol. 54, No. 6, 2516–2526, 2006.
  11. Hong, J.-S., *Wiley Series in Microwave and Optical Engineering, Microstrip Filters for RF/Microwave Applications*, John Wiley & Sons, Inc., 2011.
  12. Radant MEMS, MA, USA, RMSW221 SPDT RF MEMS switch (datasheet), 2 pages,[Online] Cited 2015-09-01. Available at: <http://www.radantmems.com/radantmems.data/Library/RMSW221.pdf>.